Impacts of climate changes on the phytoplankton biomass of the Indonesian Maritime Continent

Eko Siswanto [a,*], Takanori Horii [b], Iskhaq Iskandar [c], Jonson Lumban Gaol [d], Riza Yuliratno Setiawan [e], R. Dwi Susanto [f,g]

[a] Earth Surface System Research Center, Research Institute for Global Change, Japan Agency for Marine-Earth Science and Technology, 3173-25, Showa-machi, Kanazawa-ku, Yokohama, Kanagawa 236-0001, Japan
[b] Global Ocean Observation Research Center, Research Institute for Global Change, Japan Agency for Marine-Earth Science and Technology, 2-15, Natsushima-cho, Yokosuka, Kanagawa 237-0061, Japan
[c] Faculty of Mathematics and Natural Sciences, Sriwijaya University, Jl. Masjid Al Gazali, Bukit Lama, Palembang 30128, Indonesia
[d] Faculty of Fisheries and Marine Science, IPB University, Jl. Rasamala, IPB Darmaga Campus, Bogor 16680, Indonesia
[e] Faculty of Agriculture, Gadjah Mada University, Jl. Flora, Bulaksumur, Daerah Istimewa Yogyakarta 55281, Indonesia
[f] Department of Atmospheric and Oceanic Science, University of Maryland, College Park, MD 20742, USA
[g] Faculty of Earth Sciences and Technology, Bandung Institute of Technology, Jl. Ganesha 10, Bandung 40132, Indonesia

ARTICLE INFO

ABSTRACT

We used more than two decades (1997–2019) of satellite-estimated phytoplankton chlorophyll-a concentration (Chl-a) during September–December time intervals to discern the spatial and temporal changes of phytoplankton biomass in the Indonesian Maritime Continent (IMC) associated with different climatic events. In the IMC coastal areas (except for the northern Malacca Strait) climate changes influenced Chl-a by varying rainfall/river discharge. Chl-a declined most notably during concurrent positive Indian Ocean Dipole (IOD) and El Niño events, whereas they increased most notably during concurrent negative IOD and La Niña events. In the open ocean areas of the IMC, climate changes influenced Chl-a by varying the occurrence of upwelling and downwelling. The dominant climate mode determining Chl-a shifted from the IOD in the eastern Indian Ocean to the El Niño/Southern Oscillation (ENSO) in the western Pacific Ocean. In the eastern Indian Ocean, the impact of the IOD on Chl-a was more than one order of magnitude greater than the impact of ENSO. The results implied that low-trophic-level marine organisms such as phytoplankton, high-trophic-level marine organisms such as fish, and biogeochemical cycles in the eastern Indian Ocean of the IMC may all be more affected by the IOD than by the ENSO.

1. Introduction

The impact of global climate change on phytoplankton biomass is one of the most important metrics of global climate change effects because phytoplankton are the first trophic level, and from them both material and energy are transferred to higher-trophic-level organisms such as fishes. Phytoplankton are especially important in regions of the ocean where the food web is subject to bottom-up control. Phytoplankton also control important ocean biogeochemical processes such as carbon sequestration because of their role in the biological pump.

The Indonesian Maritime Continent (IMC) has been greatly affected by climate change, and within the IMC variations of phytoplankton

biomass largely control variations of fish catches (Susanto et al., 2001; Susanto et al., 2006; Iskandar et al., 2009; Sartimbul et al., 2010; Siswanto, 2015; Sari et al., 2020). This sensitivity to climate change reflects the fact that the IMC is situated between the Indian and Pacific Oceans, where the Indian Ocean Dipole (IOD) and the El Niño/Southern Oscillation (ENSO) occur, respectively. Previous studies, however, have focused on specific areas within the IMC and have analyzed climate events when both IOD and ENSO events co-occurred, such as 1997 and 2006, when a positive IOD coincided with an El Niño.

The impacts of single climate events (i.e., a single IOD or a single ENSO event) and concurrent IOD and ENSO events on phytoplankton biomass over the entire IMC are therefore not well documented. Which

---

climate mode has a greater impact on the phytoplankton community over the entire IMC, particularly during concurrent IOD and ENSO events, is also unclear.

In this study, we used more than two decades of satellite-derived chlorophyll-a concentration (Chl-a, mg m^{-3}), a measure of phytoplankton biomass, to discern the impact of different climate events on the Chl-a in the IMC and to identify the climate event that primarily influences Chl-a. Based on our findings, we discuss the probable underlying physical mechanism(s).

2. Methodology

2.1. Study area

The IMC extends from 92°E to 149°E and from 14°S to 13°N. It encompasses the equatorial seas from the eastern Indian Ocean (west of Sumatra) to the westernmost Pacific Ocean north of Papua, and from the Indian Ocean south of Java to the southern South China Sea (Fig. 1).

The study area included coastal, shelf, and deep seas within the IMC and was selected based on its biogeophysical sensitivity to climate variability in both the Indian and Pacific Oceans (Susanto et al., 2001; Wilson and Adamec, 2001; Iskandar et al., 2009; Sartimbul et al., 2010; Siswanto, 2015; Siswanto et al., 2017; Sari et al., 2020). The study area also connects the tropical Indian and Pacific Oceans via the Indonesian throughflow and the various passages of the Sunda archipelago (e.g., Sprintall et al., 2014). Because the IMC has an extremely long coastline, it is also greatly influenced by river systems.

2.2. Data sources and analysis

Merged monthly Chl-a data from September 1997 to December 2019 (4-km spatial resolution) retrieved by multiple ocean colour sensors were acquired from the Ocean Colour-Climate Change Initiative (OC-CCI) project website (https://esa-oceancolour-cci.org/). To assess the magnitude of upwelling/downwelling (a proxy for nutrient input from subsurface waters), we acquired monthly sea surface height anomaly

(SSHA, m) data with a 25-km spatial resolution observed by multiple satellite altimetry from the AVISO+ Satellite Altimetry Data (https://www.aviso.altimetry.fr/).

We also used in situ vertical profiles of salinity measured by Argo floats to confirm the occurrence of upwelling/downwelling in the eastern Indian Ocean west of Sumatra. The Argo data were obtained from the advanced automatic quality control Argo Data prepared by the Japan Agency for Marine-Earth Science and Technology (http://www.jamstec.go.jp/ARGO/argo_web/argo/?page_id=100&lang=en). As a proxy for riverine nutrient load, we used modeled monthly river discharge (m^3 s^{-1}) data (downloaded from https://www.eorc.jaxa.jp/water/) and merged monthly rainfall (mm d^{-1}) data observed by multiple platforms and downloaded from the Climate Prediction Center Merged Analysis of Precipitation (https://www.esrl.noaa.gov/psd/data/gridded/data.cmap.html).

Rivers supply not only nutrients but also suspended matter and dissolved organic matter. Large amounts of these substances in the water are well known to cause overestimation of satellite Chl-a retrieved on the basis of the blue-to-green waveband ratio. To assess the spatial extent of suspended matter and dissolved organic matter that might influence satellite Chl-a, we also analyzed normalized water-leaving radiance at 555 nm (nLw$_{555}$, mW cm^{-2} μm^{-1} sr^{-1}) and the detritus/gelbstoff absorption coefficient at 443 nm (adg$_{443}$, m^{-1}). The nLw is a product of remote sensing reflectance and the mean nominal band solar irradiance. We also downloaded remote sensing reflectance and adg$_{443}$ data from the OC-CCI project website.

The IOD and ENSO are interannual climate phenomena. Therefore, before we assessed the association between biogeophysical variables and climate variations, we removed the seasonality of the biogeophysical variables by subtracting the monthly climatological means from the time series of biogeophysical data and then removed the long-term trends. To identify ENSO events, we used NINO3.4 sea surface temperature anomaly data (NINO3.4), which were downloaded from http://www.cpc.ncep.noaa.gov/data/indices/sstoi.indices. We used Dipole Mode Index (DMI) data downloaded from http://www.jamstec.go.jp/aplinfo/sintexf/iod/dipole_mode_index.html to identify IOD
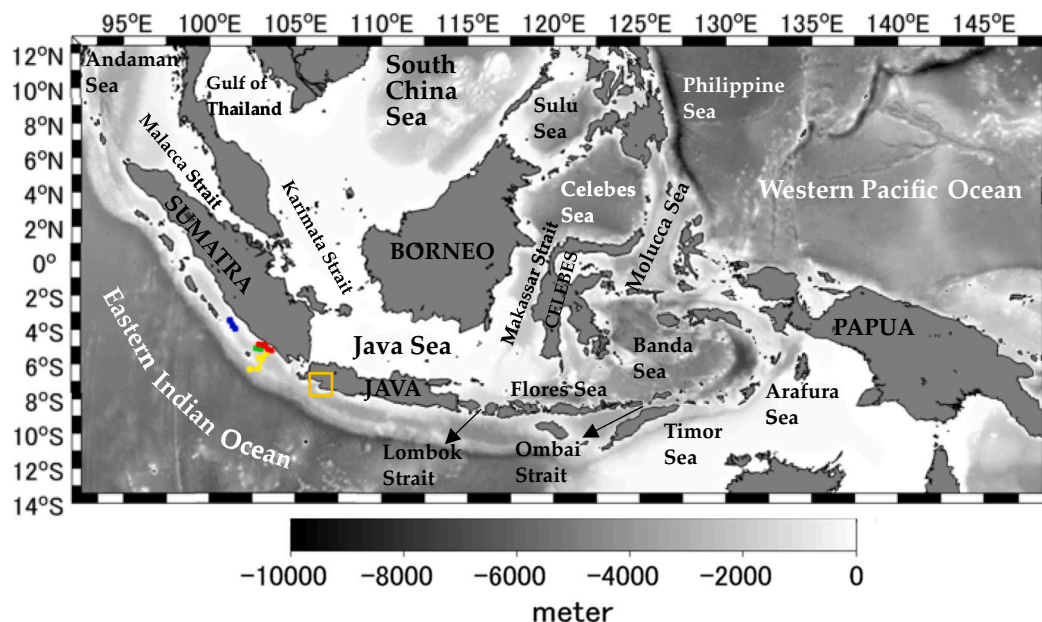

Fig. 1. Bathymetric map of the study area, which is bounded by latitudes of 14°S and 13°N and longitudes of 92°E and 149°E. The study area encompasses the equatorial seas from the eastern Indian Ocean (west of Sumatra) to the westernmost Pacific Ocean north of Papua, and from the Indian Ocean south of Java to the southern South China Sea. Gray shading indicates bottom depths in negative meters. The green, red, blue, and yellow marks are trajectories of Argo floats that measured salinity from 28 September to 7 November 2013, 5 October to 14 November 2015, 23 July to 1 September 2016, and 16 August to 25 September 2017, respectively. The orange square indicates the location of Pelabuhan Ratu Bay, West Java, where in situ Chl-a data were collected during the 5 October 2019 field observations. (For interpretation of the references to colour in this figure legend, the reader is referred to the web version of this article.)

events.

The impacts of the IOD and ENSO on Chl-a were investigated with three approaches: by relating Chl-a with climate indices (NINO3.4 and DMI) using Pearson correlation analysis (e.g., Siswanto et al., 2017), by composite analysis (averaging all Chl-a data during the years of each climate event), and by observing the temporal variation of spatially averaged Chl-a from 1997 to 2019, but only for the months of September to December. Temporal variations of mean Chl-a were derived for the main sub-areas after elimination of the possible influences of total suspended and dissolved organic matters, especially in the coastal areas, as will be detailed in Section 3. Pearson correlation analysis was also conducted to see the relationships between Chl-a and other variables in the main sub-areas. The significance levels ($p < 0.05$, $p < 0.01$, and $p < 0.001$) of the correlations will be shown when discussing the coefficient of correlation (r).

Composite analysis was performed on Chl-a data for the periods of single positive IOD (+sIOD), single negative IOD (−sIOD), single El Niño (sEN), single La Niña (sLN), concurrent +IOD and El Niño (+IOD_EN), and concurrent −IOD and La Niña (−IOD_LN) events. Note that in this study +sIOD, −sIOD, sEN, and sLN refer to a single climate event that happened in a particular year, and +IOD, −IOD, EN, and LN refer to climate events in a general sense. An EN (LN) event was considered to have occurred if the NINO3.4 was higher (lower) than 0.5 (e.g., Butler and Polvani, 2011). A +IOD (−IOD) event was considered to have occurred if the DMI was higher (lower) than one DMI standard deviation (e.g., Iskandar et al., 2013). Also, to capture usual IOD and ENSO (whether concurrent or single) events, we used another criterion, so that the thresholds of IOD and ENSO mentioned above can be observed from September to December. There have been some years with unusual short-lived +IOD event that has occurred in summer followed by LN event that has occurred in fall or winter (e.g., Behera et al., 2008; Horii et al., 2013; Iskandar et al., 2013; Zhang et al., 2018). We classified those years as +IOD_LN event.

Based on the above criteria, from the more than two decades of satellite-derived Chl-a data, we were able to identify years with distinctly different climate events: neutral condition (2001, 2003, and 2013), +IOD_EN event (1997, 2006, and 2015), −IOD_LN event (1998 and 2010), +sIOD event (2012 and 2019), −sIOD event (2016), sEN event (2002, 2004, and 2009), sLN event (1999 and 2000), and +IOD_LN event (2007, 2008, 2011, and 2017) (Fig. 2). The mean Chl-a was calculated during each climate event, and the deviation of the mean Chl-a during a certain climate event from the mean Chl-a during neutral condition was interpreted as the impact of the climate event on the Chl-a in the IMC. The same approach and interpretation were applied to other geophysical variables.

Although all the variables (Chl-a, SSHA, rainfall, and river discharge) in the following discussion were deviations from mean values during neutral condition, for simplicity, we designated them as Chl-a, SSHA,

rainfall, and river discharge. Because in many cases a relationship between high Chl-a, especially in the eastern Indian Ocean, and +IOD and EN is apparent from September to December (e.g., Susanto and Marra, 2005; Iskandar et al., 2009; Siswanto, 2015), we used the mean Chl-a (as well as the mean of geophysical variables) averaged from September to December.

3. Results and discussion

3.1. Correlations between Chl-a and climate indices

The significant ($p < 0.05$) positive correlation between the DMI and Chl-a—mainly in the eastern Indian Ocean (the area extending from west of Sumatra to south of Lombok Strait) and the eastern archipelagic seas of Banda, Arafura, and Molucca (Fig. 3a)—indicated that Chl-a in those areas tended to increase during +IOD event and to decrease during −IOD event. In the same areas, positive correlations were also observed between the NINO3.4 and Chl-a (Fig. 3e), but those correlations were strongest in the Molucca Sea and the western Pacific Ocean north of Papua. These correlations indicated that Chl-a tended to increase (decrease) in those areas during EN (LN).

In contrast, associations between Chl-a and climate indices in the Sunda shelf (the Java Sea, Karimata Strait, and southernmost area of the South China Sea) were not clear. In the coastal areas surrounding Borneo and east of southern Sumatra, the inverse relationships revealed by Pearson correlation between DMI and Chl-a as well as between NINO3.4 and Chl-a indicated that Chl-a tended to decrease during +IOD and/or EN events and to increase during −IOD and/or LN events. The tendency for rainfall and river discharge to decline (indicated by the negative correlations in Fig. 3c, g and in Fig. 3d, h, respectively) might reduce riverine nutrient inputs during +IOD and/or EN events and hence might be responsible, at least in part, for the decline of Chl-a during +IOD and/or EN events in coastal areas.

The open ocean areas of the IMC were characterized by positive correlations between DMI and Chl-a as well as between NINO3.4 and Chl-a (Fig. 3a, e) and by negative correlations between DMI and SSHA as well as between NINO3.4 and SSHA (Fig. 3b, f). The negative correlations indicated a tendency for the SSHA to decrease (increase) during +IOD and/or EN (−IOD and/or LN) events. The decrease of the SSHA during +IOD and/or EN events indicated the occurrence of upwelling. The increase of Chl-a during +IOD and/or EN events in the areas where the DMI–Chl-a and NINO3.4–Chl-a correlations were positive could therefore be attributed to nutrients supplied from upwelled water (Susanto et al., 2001; Wilson and Adamec, 2001; Iskandar et al., 2009; Siswanto, 2015).

3.2. Chl-a changes during different climate events

The correlation noted in Section 3.1 between the climate index and Chl-a, however, did not reflect the impact of any single climate event (+sIOD, −sIOD, sEN, and sLN) on Chl-a because the climate indices (DMI and NINO3.4) used here included both +IOD_EN and −IOD_LN events. The implication is that the correlation between NINO3.4 (DMI) and Chl-a might be overwhelmed by the correlation between DMI (NINO3.4) and Chl-a. Furthermore, the magnitude of the correlation coefficient between Chl-a and a climate index does not provide information about the magnitude of the change of Chl-a during a climate event. The mean Chl-a during a particular climate event and how much it deviates from the mean Chl-a during neutral events can provide a metric of the magnitude of the Chl-a changes.

3.2.1. Impacts of single IOD events

3.2.1.1. +sIOD event (2012, 2019). The fact that Chl-a in the eastern Indian Ocean was higher during a +sIOD event (Fig. 4a) than during
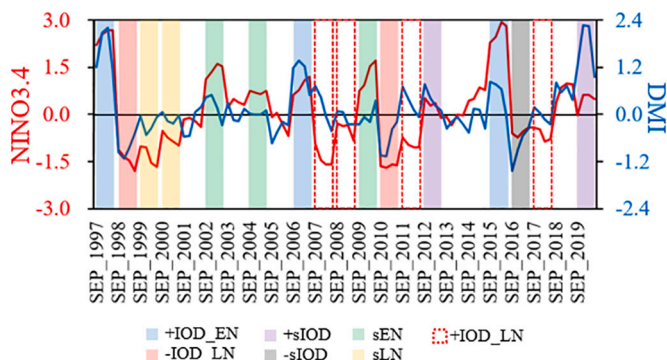

Fig. 2. Time series of NINO3.4 and DMI from September to December during the period 1997–2019. The years with the same climate events are indicated by vertical bars of the same colour.
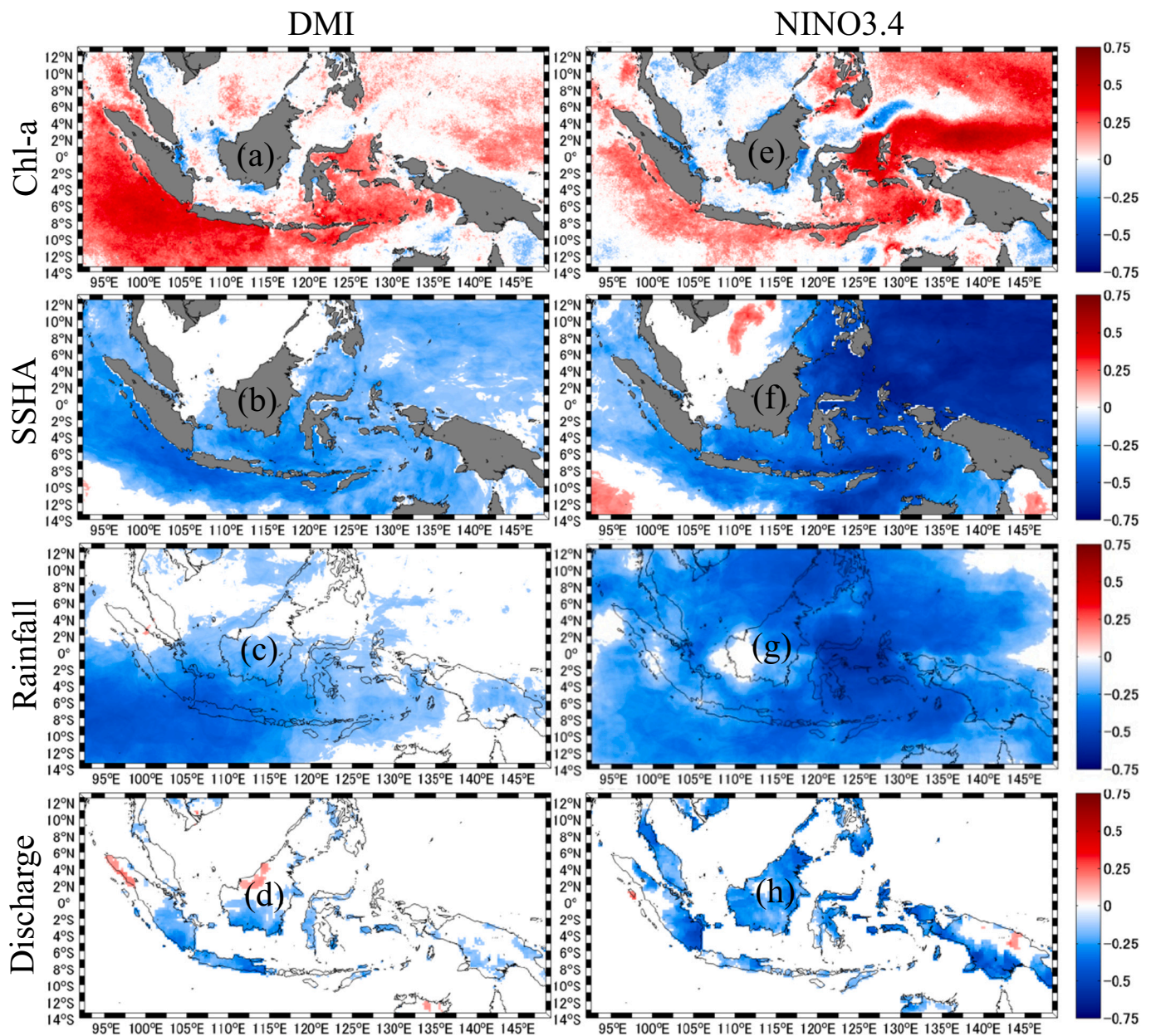
Fig. 3. Spatial variations of significant ($p < 0.05$) Pearson correlation coefficients derived by relating Chl-a (a), SSHA (b), rainfall (c), and river discharge (d) to DMI. Panels (e–h) are the same as panels (a–d), except that the correlations are versus NINO3.4. Areas with insignificant correlations are masked out (white areas). A positive correlation means that the values of the biogeophysical variable tended to be high when the climate indices were positive (i.e., during EN and/or + IOD events). Negative correlations indicate the opposite pattern.

neutral conditions was consistent with the positive correlation between DMI and Chl-a (Fig. 3a). From now on, a "high" will be used to refer to a Chl-a that was higher than the during neutral condition. A "low" will then be used to refer to a Chl-a that was lower than the during neutral condition. In the open ocean west of Sumatra and south of Java, the Chl-a can sometimes be 5.00 mg m^{-3} higher than during neutral conditions. Note that the range of the Chl-a colormap was narrowed to -0.75 to 0.75 mg m^{-3} to reveal small Chl-a variations in the western Pacific Ocean.

The 2019 +sIOD event was one of the strongest +sIOD events and comparable to the 1997 +IOD event (Fig. 2). The Chl-a southwest of Sumatra and Java that sometimes exceeded 10.00 mg m^{-3} were observed by the Sentinel-3 satellite Ocean and Land Colour Instrument on 5 October 2019 (Fig. 5a). Specifically, in Pelabuhan Ratu Bay, West Java, the satellite Chl-a greater than 10.00 mg m^{-3} was verified by Chl-a

in situ measurements also conducted on 5 October 2019. During normal condition (1–16 October 2013, Fig. 5b) the mean Chl-a southwest of Sumatra and Java and Pelabuhan Ratu Bay were only about 0.20 mg m^{-3} and 1.00 mg m^{-3}, respectively.

The high Chl-a in the eastern Indian Ocean has been attributed to upwelling caused by both remote and local forcing factors (e.g., Saji et al., 1999; Chen et al., 2016; Delman et al., 2016). Upwelling in the eastern Indian Ocean during +sIOD event was revealed by the low SSHA (Fig. 4b). To gain a quantitative understanding of Chl-a changes and the likely responsible factors, we calculated the temporal changes (i.e., time series of deviations from neutral condition) of Chl-a and other geophysical variables averaged within the polygons outlined in Fig. 10a. From now on, the discussion of the time series of Chl-a and SSHA will concern averages within the green polygons outlined in Fig. 10a, whereas for the time series of rainfall and river discharge were within
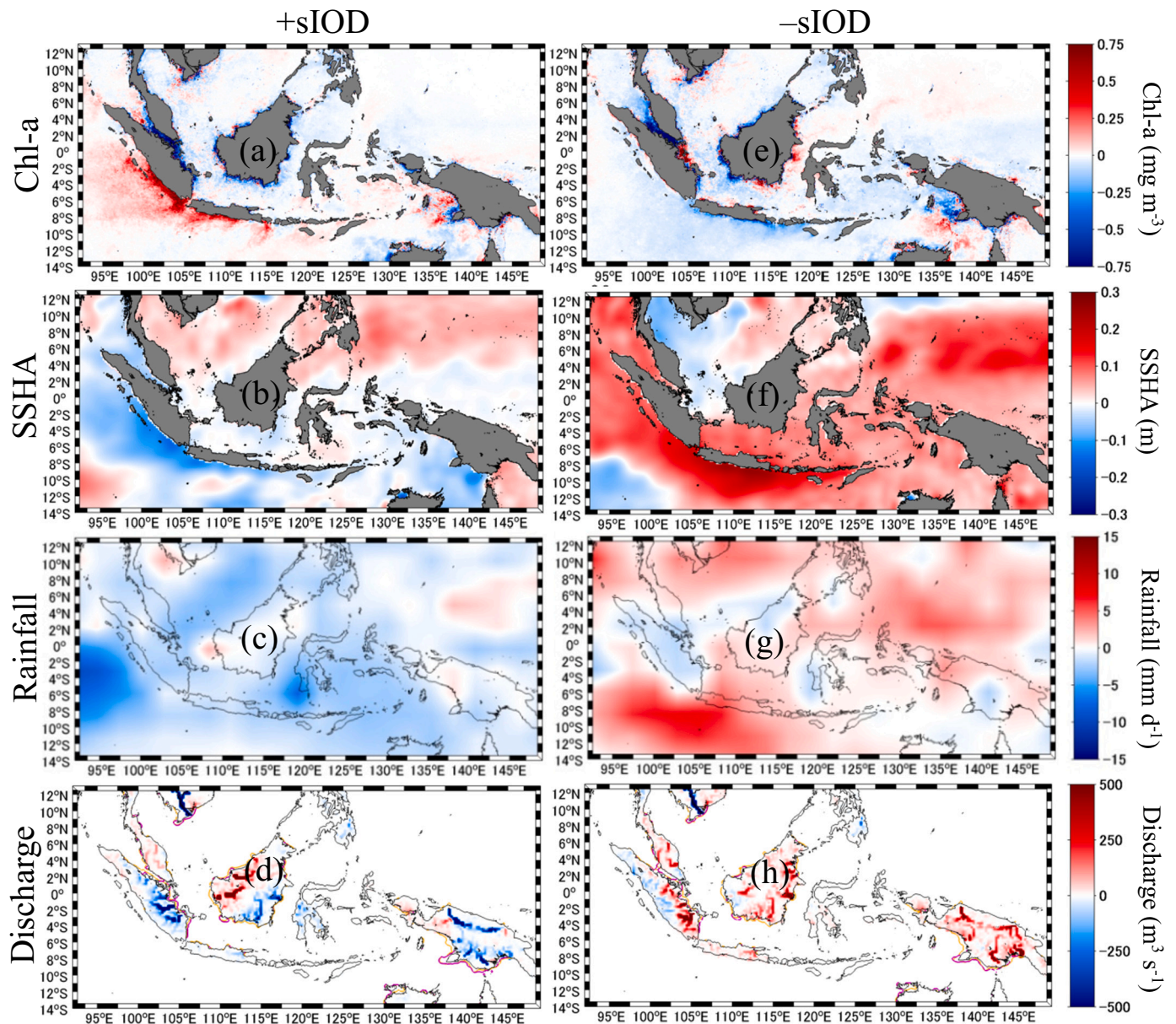
+sIOD

−sIOD

Fig. 4. (a) Map of mean Chl-a during +sIOD event averaged from September to December. The Chl-a was determined by subtracting the mean Chl-a during neutral condition (2001, 2003, and 2013) from the mean Chl-a during +sIOD event (2012 and 2019) (see the division of years based on different climate events in Fig. 2). Panels (b), (c), and (d) are the same as panel (a), but they are maps of SSHA, rainfall, and river discharge, respectively. The purple and yellow contours overlaid on the river discharge maps are nLw_{555} and adg_{443} contours with values of 2.5 mW cm^{-2} μm^{-1} sr^{-1} and 0.2 m^{-1}, respectively. Panels (e–h) are the same as panels (a–d), but they correspond to a −sIOD event (2016). (For interpretation of the references to colour in this figure legend, the reader is referred to the web version of this article.)

the red polygons.

The high Chl-a west of Sumatra and south of Java were mainly due to the strong 2019 +sIOD, as indicated by the high DMI (Fig. 2) and low SSHA (Fig. 10b, c). During the weak 2012 +sIOD, the Chl-a was not so high because the upwelling was weak. In the eastern archipelagic seas, Chl-a was 0.10–0.20 mg m^{-3} higher during +sIOD event than during neutral condition (Fig. 4a). An increase of Chl-a there has also been attributed to the eastern Indian Ocean upwelling that propagates into the Indonesian seas through the Lombok and Ombai Straits (e.g., Iskandar, 2010; Susanto et al., 2012). This association between upwelling and increased Chl-a was apparent in the Banda Sea (Fig. 10d) and Arafura Sea (Fig. 10e), particularly during the strong 2019 +sIOD. The upwelling that was the main cause of the high Chl-a from the eastern Indian Ocean to the eastern archipelagic seas and north of Papua was

consistent with the significant, negative correlations between Chl-a and SSHA ($r = -0.57$ to -0.87, $p < 0.001$; Fig. 10b–g). In the Java Sea, the correlation between Chl-a and SSHA was negative but not statistically significant (Fig. 10h).

In the coastal area east of southern Sumatra, Chl-a was about 0.50–1.00 mg m^{-3} lower during +sIOD event than during neutral condition (Fig. 4a). Note that the coastal area bordered by the green polygons (Fig. 10a) covered the areas with $nLw_{555} > 2.5$ mW cm^{-2} μm^{-1} sr^{-1} and $adg_{443} > 0.2$ m^{-1} (Fig. 4d). Tan et al. (2006) and Siswanto et al. (2011) have reported that satellite Chl-a retrieved using a standard empirical algorithm is an overestimate in the areas where nLw_{555} and adg_{443} are higher than the threshold values mentioned above. Therefore, coastal areas where $nLw_{555} > 2.5$ mW cm^{-2} μm^{-1} sr^{-1} and/or $adg_{443} > 0.2$ m^{-1} are defined as invalid areas where Chl-a data are invalid. The
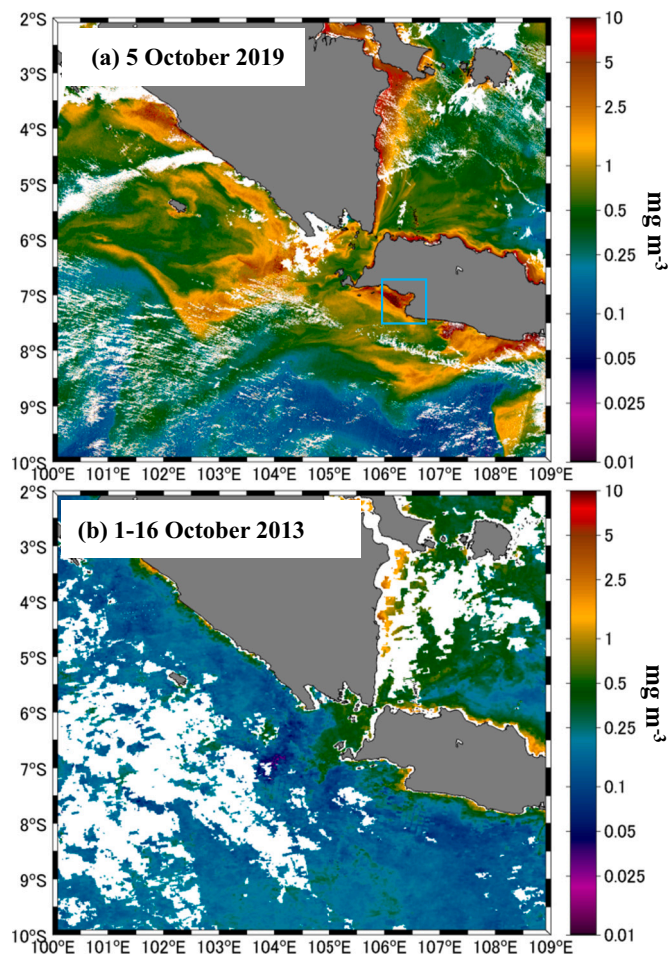
Fig. 5. (a) High-resolution (300 m) image of Chl-a southwest of Java and Sumatra observed by Ocean and Land Colour Instrument onboard the Sentinel-3 satellite on 5 October 2019 (+sIOD event). The data were downloaded from the Copernicus Online Data Access (https://coda.eumetsat.int/#/home). Blue box in (a) indicates the location of Pelabuhan Ratu Bay, where the in situ measurements of Chl-a were made on 5 October 2019. (b) A 1-km resolution image of Chl-a southwest of Java and Sumatra observed by multi-ocean colour sensors on 1–16 October 2013 (neutral condition). The data were acquired from the OC-CCI project (https://esa-oceancolour-cci.org/). (For interpretation of the references to colour in this figure legend, the reader is referred to the web version of this article.)

time series of Chl-a, especially in coastal areas, was therefore spatially averaged over the green polygons, but excluding the invalid areas. After the invalid areas were excluded, the decline of Chl-a east of southern Sumatra was prominent, especially during the strong 2019 +sIOD (Fig. 11c, top panel), which seemed to be associated with declines in both rainfall and river discharge (Fig. 11c, bottom panel) over the connected land areas (see Fig. 10a). This land–ocean interaction was consistent with the overall significant, positive correlation between Chl-a and rainfall ($r = 0.42$, $p < 0.001$) and between Chl-a and river discharge ($r = 0.60$, $p < 0.001$) (Fig. 11c).

Coastal areas surrounding Borneo were also characterized by a decline of Chl-a (Fig. 4a) during this period of low rainfall (Fig. 4c, see also Nur'utami and Hidayat, 2016). Even after removing the invalid areas, Chl-a to the east (Fig. 11a, top panel), southwest (Fig. 11b, top panel), south (Fig. 11d, top panel), and northwest (Fig. 11e, top panel) of Borneo were still low, although the SSHA indicated weak upwelling (top panels of Fig. 11a, b, d, e). The lowest Chl-a (about 0.70 mg m^{-3} below the concentration associated with neutral condition) was observed to the south of Borneo during the strong 2019 +sIOD. The

decline of Chl-a there, despite the occurrence of upwelling, might have been associated with a decline in riverine nutrient inputs, as indicated by the decline of river discharge and the significant, positive correlation between Chl-a and river discharge (bottom panels in Fig. 11a, b, d, e).

In the northern Strait of Malacca, the tendency for Chl-a to increase during +sIOD event might be attributed to upwelling (Fig. 4a, b) (see also Tan et al., 2006; Siswanto and Tanaka, 2014; Siswanto, 2015). However, such an association between upwelling (low SSHA) and high Chl-a seemed to be observable only during the strong 2019 +sIOD (Fig. 11f, top panel). Upwelling seemed to be the main factor responsible for the increase of Chl-a. This conclusion was consistent with the significant, negative correlation between Chl-a and SSHA ($r = -0.47$, $p < 0.001$; Fig. 11f, top panel). The significant negative correlation between Chl-a and rainfall ($r = -0.30$, $p < 0.01$) or discharge ($r = -0.43$, $p < 0.001$) (Fig. 11f, bottom panel) suggested that input of riverine nutrients was not a determinant of the Chl-a variations in the northern Malacca Strait.

3.2.1.2. –sIOD event (2016). During the –sIOD event, the high SSHA that characterized almost all areas of the IMC indicated the occurrence of downwelling (Fig. 4f) that was responsible for the decline of Chl-a over the same areas (Fig. 4e). The associations between high SSHA and low Chl-a were apparent in the areas west of Sumatra (Fig. 10b), south of Java (Fig. 10c), the Banda Sea (Fig. 10d), the Arafura Sea (Fig. 10e), the Molucca Sea (Fig. 10f), and north of Papua (Fig. 10g). The fact that downwelling was the main cause of the Chl-a declines was consistent with the significant, negative correlation between Chl-a and SSHA in those areas ($r = -0.57$ to -0.87, $p < 0.001$; Fig. 10b–g). The Chl-a declined by 0.50 mg m^{-3} below concentration associated with neutral condition in the eastern Indian Ocean, but by only 0.05 mg m^{-3} north of Papua.

The occurrence of downwelling west of Sumatra was verified by vertical profiles of salinity measured by Argo float from 23 July to 1 September 2016 (Fig. 6a). The profiles showed strong vertical stratification and a thick salinity barrier layer, that is, the layer between the depths of the mixed layer and isothermal layer. Downwelling was stronger during the –sIOD event than during neutral condition, which was characterized by a relatively weak barrier layer recorded by Argo float from 28 September to 7 November 2013 (Fig. 6b).

In the coastal area east of southern Sumatra, satellite Chl-a (Fig. 4e) was high. However, the fact that a large portion of the region was occupied by invalid areas associated with high nLw$_{555}$ and adg$_{443}$ (Fig. 4h) due to high river discharge from the adjacent land (Figs. 4h, 11c, bottom panel) calls into question these high Chl-a. After the invalid areas were removed, the change of Chl-a was not remarkable (Fig. 11c, top panel). The coastal area south of Borneo was also largely occupied by invalid areas (Fig. 4h) associated with high rainfall and river discharge (Figs. 4g, h, 11d, bottom panel). Removing invalid areas resulted in a decline of Chl-a (Fig. 11d, top panel).

Chl-a in the coastal area east of Borneo was high during this period of above-average rainfall (Nur'utami and Hidayat, 2016) (Figs. 4e, 11a, top panel). This high Chl-a seemed to be valid because the area there included few invalid areas (Fig. 4h). The tendency of the SSHA to be high (Figs. 4f, 11a, top panel) indicated a limited vertical input of nutrients. An increase of nutrients supplied from rivers in eastern Borneo due to high river discharge (Figs. 4h, 11a, bottom panel) might thus have been among the factors responsible for the increase of Chl-a in the coastal area east of Borneo. The significant, positive correlation between Chl-a and discharge ($r = 0.33$, $p < 0.01$; Fig. 11a, bottom panel) was consistent with this land–ocean interaction.

Although both rainfall and river discharge in southwestern Borneo (Figs. 4g, h, 11b, bottom panel) tended to be high, Chl-a in the coastal area southwest of Borneo (Fig. 4e) was low, even after removal of invalid areas (Fig. 11b, top panel). The factor responsible for the decline of Chl-a is unclear because the SSHA did not change by much (Figs. 4f, 11b, top
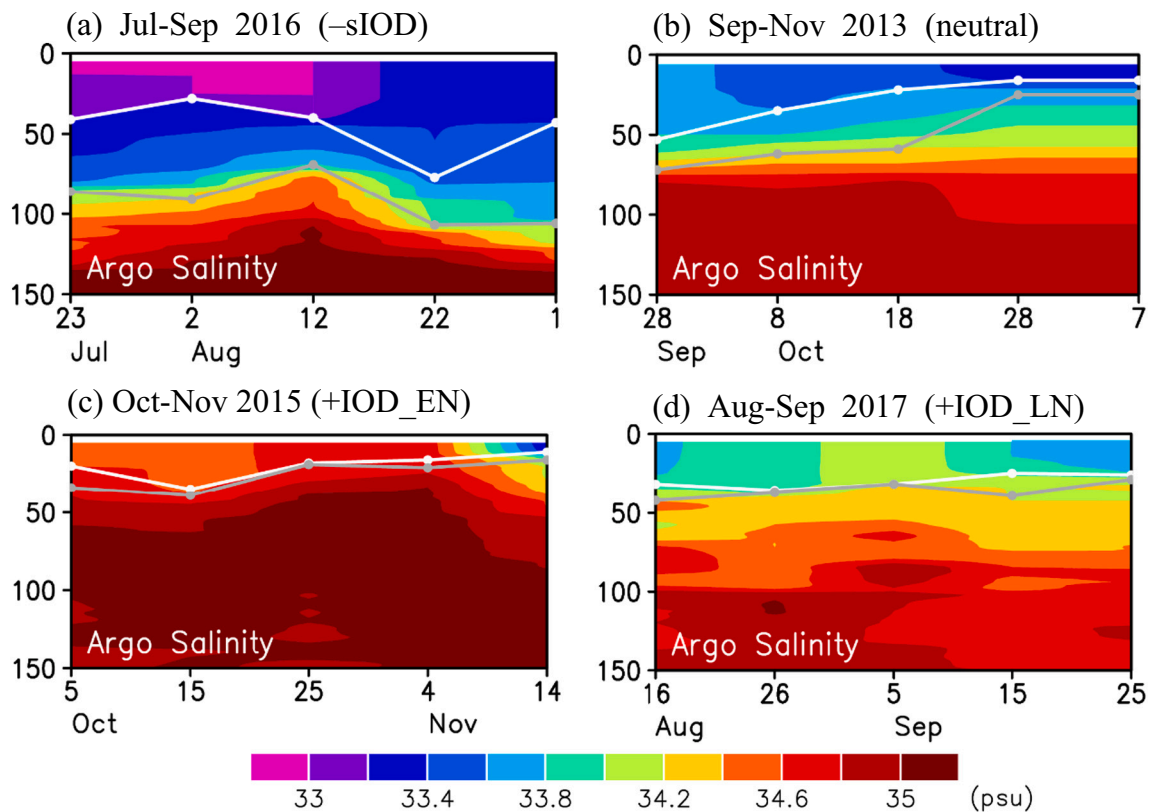
Fig. 6. Vertical profiles of salinity measured by Argo floats beneath the Argo trajectories indicated in Fig. 1. Panels (a), (b), (c), and (d) are vertical profiles of salinity measured during the –sIOD event (23 July to 1 September 2016), neutral condition (28 September to 7 November 2013), the +IOD_EN event (5 October to 14 November 2015), and the +IOD_LN event (16 August to 25 September 2017), respectively. The observations lasted 10 days in each case, and the *x*-axis indicates each date. White and gray lines indicate mixed layer depth and isothermal layer depth, respectively.

panel). In the coastal area northwest of Borneo (Figs. 4e, 11e, top panel), the Chl-a was low. The decline of riverine inputs due to lower rainfall (Figs. 4g, 11e, bottom panel) might have been responsible for decline of Chl-a there.

In the northern Malacca Strait, Chl-a (Fig. 4e) tended to be low. This pattern seemed not to be compromised by invalid areas, which were not large (Fig. 4h). Downwelling indicated by high SSHA (Figs. 4f, 11f, top panel) reduced vertical nutrient inputs and might have been responsible for the decline of Chl-a there. The significant, negative correlation between Chl-a and SSHA ($r = -0.47$, $p < 0.001$; Fig. 11f, top panel) confirmed that downwelling was an important mechanism in reducing Chl-a in the northern Malacca Strait. The role of downwelling in depressing Chl-a in the northern Malacca Strait was mentioned previously by Tan et al. (2006).

3.2.2. Impacts of single ENSO events

3.2.2.1. sEN event (2002, 2004, and 2009). During sEN event, Chl-a over most of the IMC was high, except in coastal areas (Fig. 7a). The increase of Chl-a in the open ocean areas was caused by upwelling, as evidenced by the low SSHA over the entire IMC (Fig. 7b). Time series data revealed associations between upwelling and high Chl-a over vast areas from the eastern Indian Ocean to the western Pacific Ocean (Fig. 10b–g). These associations between upwelling and high Chl-a were consistent with the significant, negative correlations between Chl-a and SSHA ($r = -0.57$ to -0.87, $p < 0.001$; Fig. 10b–g). The association between upwelling and high Chl-a was also observed in the Java Sea, although the correlation coefficient between Chl-a and SSHA was not significant ($r = -0.18$, $p > 0.05$; Fig. 10h).

The highest increase of Chl-a (about 0.40 mg m^{-3} higher than the concentration under neutral condition) was observed in the Arafura Sea

because of strong upwelling (Fig. 10e). Strong upwelling north of Papua was also observed, but Chl-a increased by only 0.03 mg m^{-3} (Fig. 10g), even though the correlations between NINO3.4 and Chl-a as well as between NINO3.4 and SSHA (Fig. 3e, f) were the highest there. Wilson and Adamec (2001) also noted an increase of Chl-a due to upwelling north of Papua during a sEN event.

Shoaling of the thermocline in the eastern Indian Ocean due to relatively cold waters transported by the Indonesian throughflow from the Pacific to the Indian Ocean (Susanto et al., 2001) and Rossby wave propagation from the Pacific Ocean to the archipelagic seas as an upwelling coastal Kelvin wave along the west coast of Papua (Iskandar, 2010) are physical oceanographic mechanisms that explain the upwelling throughout most of the IMC during sEN events.

Although low SSHA suggested the occurrence of upwelling (Fig. 7b), Chl-a in the coastal areas surrounding Borneo and east of southern Sumatra was low (Fig. 7a), even after removal of invalid areas (Fig. 11a–e, top panels). A reduction of riverine nutrient inputs due to lower rainfall and/or river discharge in the connected lands (Figs. 7c, d, 11a–e, bottom panels) was likely among the factors that caused the decline of Chl-a. The implication is that, among the interannual variations related to low rainfall during sEN event (Nur'utami and Hidayat, 2016), changes in the fluxes of nutrients from rivers are more important than changes in upwelled nutrient fluxes in determining variations of Chl-a, as previously noted by Siswanto et al. (2017) and Sun (2017). This land–ocean interaction was supported by the significant, positive correlations between Chl-a and river discharge ($r = 0.22$ to 0.60, $p < 0.01$ or <0.001; Fig. 11a–e). The most pronounced Chl-a declines (about 0.60 mg m^{-3} below concentration associated with neutral condition) were observed in the coastal areas east of southern Sumatra and south of Borneo (Fig. 11c, d, top panels).

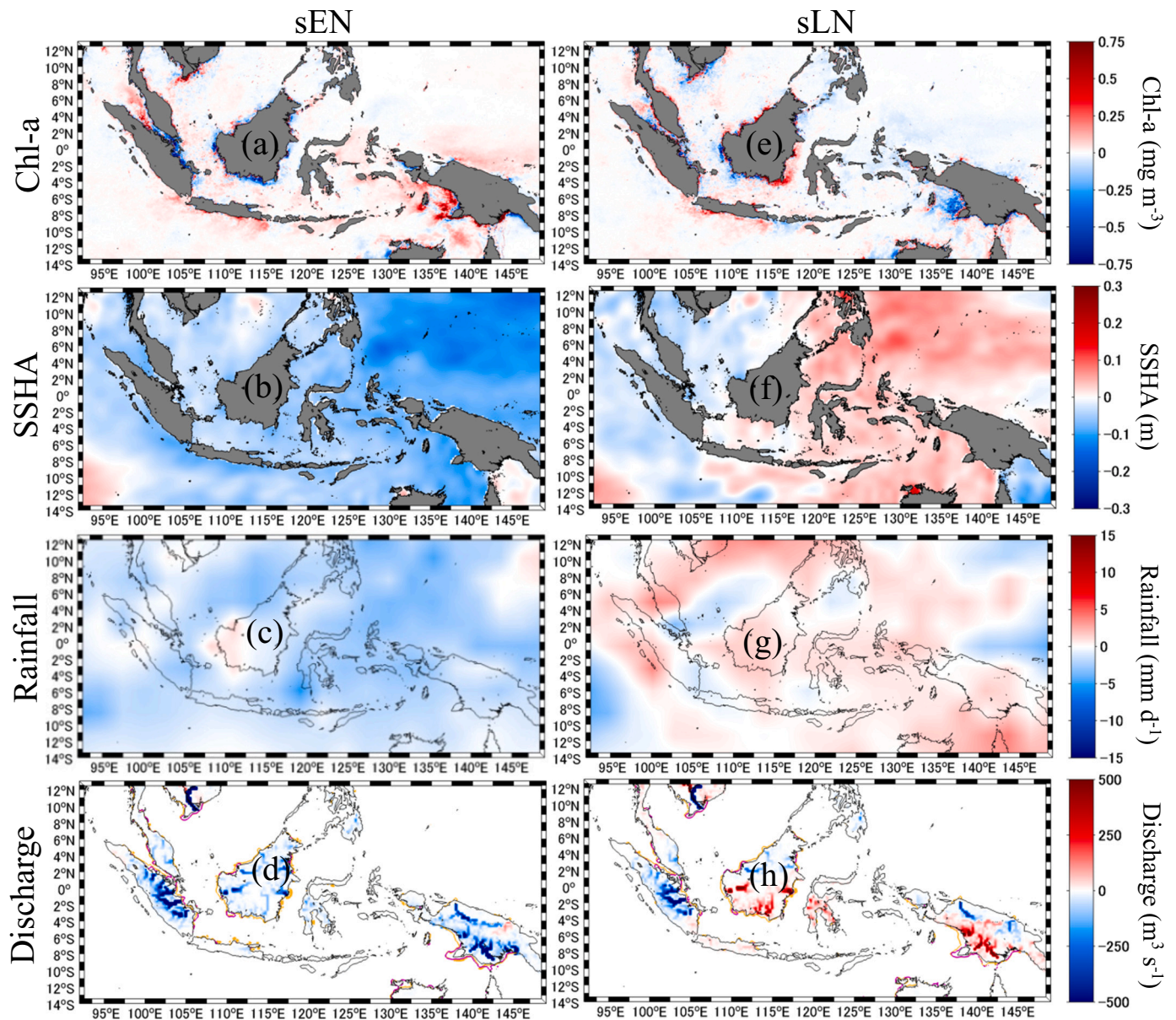In the northern Malacca Strait, although rainfall and river discharge

Fig. 7. (a) Map of mean Chl-a during sEN event averaged from September to December. The Chl-a was calculated by subtracting the mean Chl-a during neutral condition (2001, 2003, and 2013) from the mean Chl-a during sEN event (2002, 2004, and 2009) (see division of years based on different climate events in Fig. 2). Panels (b), (c), and (d) are the same as panel (a), but they are maps of SSHA, rainfall, and river discharge, respectively. The purple and yellow contours overlaid on the river discharge maps are nLw_{555} and adg_{443} contours with values of 2.5 mW cm^{-2} μm^{-1} sr^{-1} and 0.2 m^{-1}, respectively. Panels (e–h) are the same as panels (a–d), but they correspond to sLN events (1999 and 2000). (For interpretation of the references to colour in this figure legend, the reader is referred to the web version of this article.)

in the connected lands were low (Figs. 7c, d, 11f, bottom panel), Chl-a was about 0.20 mg m^{-3} higher (Figs. 7a, 11f, top panel) during sEN event than during neutral condition. Thus, in contrast to other coastal areas, vertical inputs of nutrients due to upwelling were more important than fluxes of nutrients from rivers in determining variations of Chl-a in the northern Malacca Strait during sEN events. This mechanism was consistent with the significant, negative correlation between Chl-a and SSHA ($r = -0.47$, $p < 0.001$; Fig. 11f, top panel).

3.2.2.2. sLN event (1999 and 2000). In general, spatial variation of Chl-a during sLN event was less distinct from that during sEN event (Fig. 7a, e). A composite analysis revealed high Chl-a south of Java that was likely caused by an increase of Chl-a during the 1999 sLN event (Fig. 10c). Furthermore, the increase of Chl-a (about 0.40 mg m^{-3} higher than neutral condition) was likely due to weak upwelling. Downwelling

and low Chl-a associations tended to be more remarkable in the eastern archipelagic seas than in the eastern Indian Ocean. These associations between downwelling and low Chl-a contributed to the significant, negative correlations between Chl-a and SSHA from the eastern Indian Ocean to the eastern archipelagic seas ($r = -0.57$ to -0.87, $p < 0.001$; Fig. 10b–g). The high Chl-a in the coastal region east of Borneo (Fig. 7e) seemed to be valid because there were few invalid areas in that region (Fig. 7h). Especially during the 1999 sLN event, the Chl-a increased by a maximum of about 0.30 mg m^{-3} above the concentration associated with neutral condition (Fig. 11a, top panel). Positive SSHA (Figs. 7f, 11a, top panel) indicated that vertical nutrient input was probably not the factor responsible for increased Chl-a. The likely cause was riverine nutrient inputs, because river discharge over eastern Borneo was high (Fig. 11a, bottom panel). In the coastal areas south and northwest of Borneo, Chl-a

was high only during the strong 1999 sLN event, which was associated with high rainfall and river discharge (Fig. 11d, e, bottom panels). The fact that high Chl-a concentrations to the east, south, and northwest of Borneo were associated with high river discharge during sLN events was also consistent with the significant, positive correlation between Chl-a and discharge ($r = 0.22$ to 0.44, $p < 0.01$ or < 0.001; Fig. 11a, d, e).

Despite heavy rainfall and high river discharge (Fig. 7g, h), Chl-a southwest of Borneo was low (Fig. 7e), even after removal of invalid areas (Fig. 11b, top panel), a conclusion also revealed by composite analysis. The high Chl-a in the northern Malacca Strait was associated with low SSHA (Fig. 11f, top panel). In contrast, the low Chl-a in the coastal area east of southern Sumatra was attributable to low river discharge (Fig. 11c) that was consistent with the significant, positive correlation between Chl-a and river discharge ($r = 0.60$, $p < 0.001$;

Fig. 11c, bottom panel).

3.2.3. Impacts of concurrent IOD and ENSO events

3.2.3.1. +IOD_EN event (1997, 2006, and 2015). Chl-a concentrations in the eastern Indian Ocean and the eastern archipelagic seas were very high (Fig. 8a), indeed much higher than during +sIOD or sEN event (Figs. 4a, 7a). On average, Chl-a in the open ocean west of Sumatra, south of Java, the Banda Sea, the Arafura Sea, and the Molucca Sea reached 0.70, 2.00, 0.15, 0.70, and 0.25 mg m^{-3}, respectively, concentrations that were higher than during neutral condition (Fig. 10b–f). The greater increase of Chl-a in the eastern Indian Ocean and archipelagic seas was attributable to stronger upwelling during +IOD_EN event (Fig. 8b) than during +sIOD or sEN event (Figs. 4b, 7b). Vertical profiles
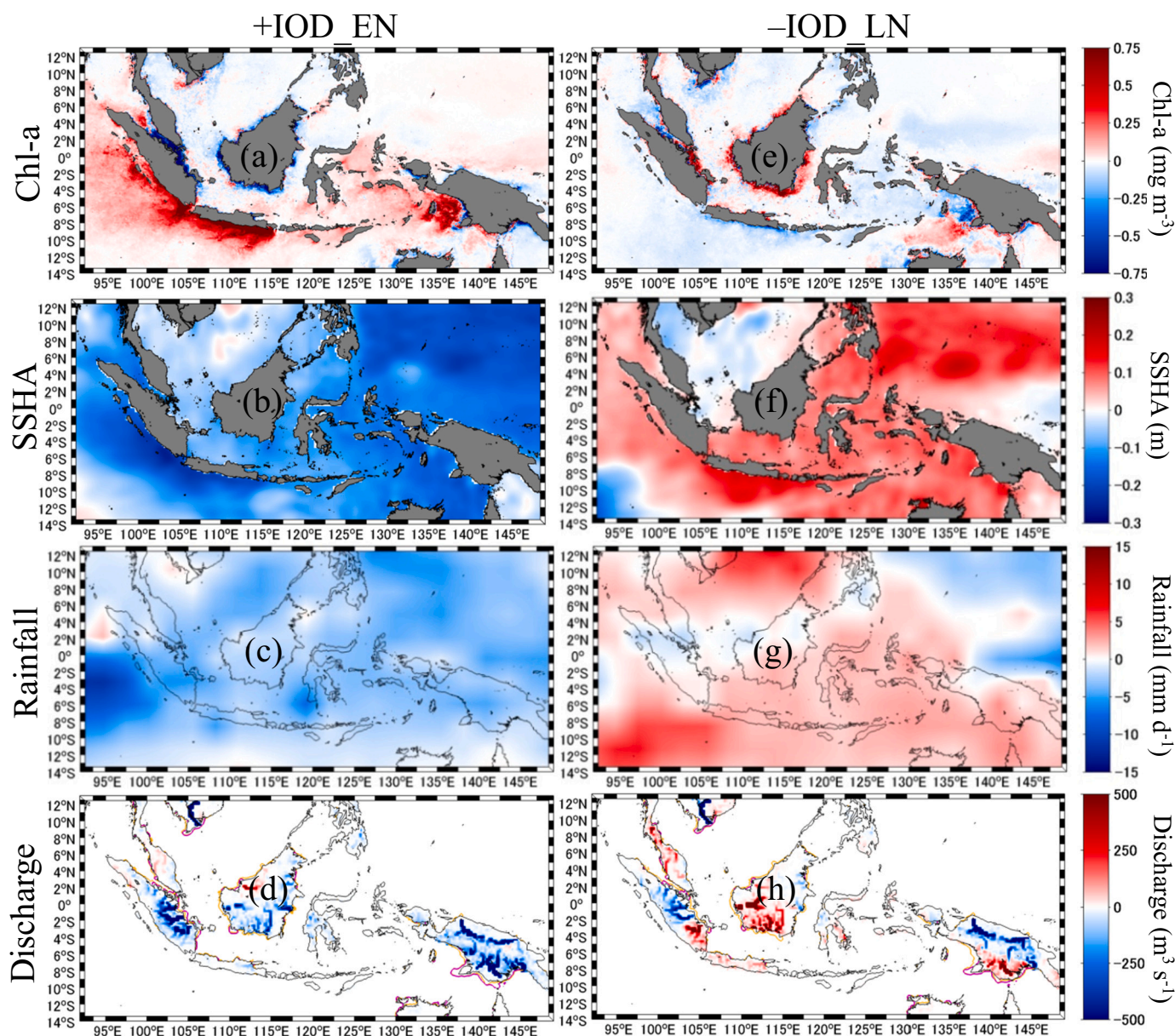

Fig. 8. (a) Map of mean Chl-a during +IOD_EN event averaged from September to December. The Chl-a was calculated by subtracting the mean Chl-a during neutral condition (2001, 2003, and 2013) from the mean Chl-a during +IOD_EN event (1997, 2006, and 2015) (see division of years based on different climate events in Fig. 2). Panels (b), (c), and (d) are the same as panel (a), but they are maps of SSHA, rainfall, and river discharge, respectively. The purple and yellow contours overlaid on the river discharge maps are nLw$_{555}$ and adg$_{443}$ contours with values of 2.5 mW cm^{-2} μm^{-1} sr^{-1} and 0.2 m^{-1}, respectively. Panels (e–h) are the same as panels (a–d), but they correspond to −IOD_LN events (1998 and 2010). (For interpretation of the references to colour in this figure legend, the reader is referred to the web version of this article.)

of salinity measured by Argo float from 5 October to 14 November 2015 revealed a very strong upwelling that was reflected by an almost uniform, high-salinity profile and colocation of the mixed layer depth and isothermal layer depth (Fig. 6c).

The combined effects of upwelling Kelvin waves, anomalous southeasterly winds (associated with +IOD event), and thermocline shoaling due to the colder water that was transported by the Indonesian throughflow (associated with EN event) strengthened the upwelling west of Sumatra and south of Java during +IOD_EN event (Saji et al., 1999; Susanto et al., 2001; Ningsih et al., 2013; Chen et al., 2016; Delman et al., 2016). Stronger upwelling in the eastern archipelagic seas was due to the combined effects of the propagation of an upwelling Kelvin wave through the Lombok and Ombai Straits (associated with +IOD event) and an upwelling Rossby wave (associated with EN event) that was propagated from the Pacific Ocean to the eastern archipelagic seas as an upwelling coastal Kelvin wave along the west coast of Papua (Iskandar, 2010; Susanto et al., 2012). Despite strong upwelling, the magnitude of the Chl-a increase was much smaller in the western Pacific Ocean north of Papua (Fig. 10g) than in the eastern Indian Ocean and the eastern archipelagic seas. The significant, negative correlations between Chl-a and SSHA ($r = -0.57$ to -0.87, $p < 0.001$; Fig. 10b–g) supported the hypothesis that upwelling was the main cause of the Chl-a increases over a vast area from west of Sumatra to north of Papua. An association between upwelling and increases of Chl-a was also observed in the Java Sea, although the overall correlation between Chl-a and SSHA was not statistically significant ($r = -0.18$, $p > 0.05$; Fig. 10h).

After removal of invalid areas, Chl-a in the coastal areas east of Borneo, southwest of Borneo, east of southern Sumatra, south of Borneo, and northwest of Borneo declined as much as 0.30, 0.40, 1.10, 0.70, and 0.30 mg m^{-3}, respectively, below the concentration associated with neutral condition, though upwelling evidenced by low SSHA seemed to be occurring in those coastal areas (Fig. 11a–e, top panels). During +IOD_EN event, the combined impacts (less rainfall) of +IOD and EN event caused a greater reduction of rainfall over the IMC (Fig. 8c) and reduction of river discharge (hence a reduction of riverine nutrient supply) into those coastal areas (Fig. 8d) (see also As-syakur et al., 2014; Nur'utami and Hidayat, 2016). The much lower rainfall and river discharge (Fig. 11a–e, bottom panels) during +IOD_EN event versus other climate events were thus likely responsible for the much low Chl-a in these areas. The significant, positive correlations ($r = 0.22$ to 0.60, $p < 0.01$ or < 0.001; Fig. 11a–e) between Chl-a and river discharge in the coastal areas east of southern Sumatra and surrounding Borneo indeed suggest that the declines of Chl-a during +IOD_EN events were attributable to decreased river discharge.

In contrast to other coastal areas surrounding Borneo and east of southern Sumatra, Chl-a in the northern Malacca Strait increased by about 0.10 mg m^{-3} above the concentration associated with neutral condition (Figs. 8a, 11f, top panel), especially during the 1997 and 2006 +IOD_EN events. Those increases were attributable to strong upwelling evidenced by the very low SSHA (Figs. 8b, 11f, top panel). Therefore, in contrast to other coastal areas where riverine nutrient inputs are more important, in the northern Malacca Strait, upwelled nutrients are more important in determining interannual variation of Chl-a related to +IOD_EN events. This mechanism was supported by the significant, negative correlation between Chl-a and SSHA ($r = -0.47$, $p < 0.001$; Fig. 11f, top panel).

3.2.3.2. –IOD_LN event (1998 and 2010). During –IOD_LN event, Chl-a in the eastern Indian Ocean and the eastern archipelagic seas declined (Fig. 8e), and the magnitudes of the declines were comparable to those during –sIOD event (Fig. 4e). The strengths of downwelling during –IOD_LN event (Fig. 8f) and –sIOD event (Fig. 4f) were also comparable. The similar spatial pattern of the declines (increases) of Chl-a (SSHA) in the open ocean areas during –IOD_LN and –sIOD events (Figs. 4e, f, 8e, f), in contrast to the tendency of Chl-a to increase during sLN event

(Fig. 7e), thus suggest that the decline of Chl-a during –IOD_LN event was due mainly to the impact of the –sIOD. Time series data clearly revealed the inverse relationship between Chl-a (low) and SSHA (high) in the open ocean from west of Sumatra to the north of Papua (Fig. 10b–g) suggesting that downwelling reduced vertical nutrient inputs and hence declined Chl-a. This mechanism was confirmed by the significant, negative correlations between Chl-a and SSHA over the vast area from west of Sumatra to the north of Papua. The most obvious Chl-a decline was observed in the Arafura Sea, where Chl-a reached 0.34 mg m^{-3} (Fig. 10e) below the concentration associated with neutral condition. The smallest decline of Chl-a was to the north of Papua (0.05 mg m^{-3}, Fig. 10g).

The combined effects of increased rainfall caused by –IOD and LN events (see As-syakur et al., 2014; Nur'utami and Hidayat, 2016) would increase river discharge and riverine nutrient supplies—though not throughout the IMC—into coastal areas much more during –IOD_LN event (Fig. 8g, h) than during –sIOD or sLN event (Figs. 4g, h, 7g, h). As a result, the increases of Chl-a in coastal areas, with the exception of the northern Malacca Strait, during –IOD_LN event were more noteworthy and occurred within a larger area (Fig. 8e) than during –sIOD or sLN event (Figs. 4e, 7e). Even after removal of invalid areas associated with high nLw$_{555}$ and adg$_{443}$ (Fig. 8h), increases of Chl-a were still apparent in the coastal areas east of Borneo, southwest of Borneo, east of southern Sumatra, south of Borneo, and northwest of Borneo (Fig. 11a–e, top panels). The attribution of those increases to river discharge (Fig. 11a–e, bottom panels) was supported by the significant, positive correlations between Chl-a and river discharge ($r = 0.22$ to 0.60, $p < 0.01$ or < 0.001). In contrast, the low Chl-a in the northern Malacca Strait was attributable to downwelling that was evidenced by high SSHA (Figs. 8e, f, 11f, top panel).

3.2.4. +IOD_LN event (2007, 2008, 2011, and 2017)

The composite analysis revealed high Chl-a over a large portion of the IMC during +IOD_LN event (Fig. 9a), especially in the eastern Indian Ocean. That high Chl-a was likely attributable to weak upwelling that was evidenced by low SSHA (Fig. 9b). The upwelling in the eastern Indian Ocean was also revealed by vertical profiles of salinity west of Sumatra measured by Argo float during 16 August to 25 September 2017 (Fig. 6d). Those profiles revealed an uplifting of high-salinity water and the colocation of the mixed layer depth and isothermal layer. High Chl-a and low SSHA in the eastern Indian Ocean were apparent mainly in the areas west of Sumatra and south of Java, particularly during 2007 and 2011. The maximum increase was about 0.40 mg m^{-3} above the concentration associated with neutral condition (Fig. 10b, c). In the western Pacific Ocean north of Papua, in contrast, Chl-a was low because of downwelling (Fig. 9a, b). The decline of Chl-a north of Papua was only about 0.05 mg m^{-3} below the concentration associated with neutral condition (Fig. 10g).

Compared to other climate events, the spatiotemporal changes of Chl-a in the coastal areas during +IOD_LN event was less uniform (Figs. 9a, 11b–f, top panels), except to the east of Borneo, where Chl-a was consistently low during all +IOD_LN event (Fig. 11a, top panel). The decline of Chl-a in the coastal area east of Borneo was not an artifact because there were relatively few invalid areas associated with high nLw$_{555}$ and ag$_{443}$ (Fig. 9d). However, the relationship between Chl-a and rainfall and/or river discharge was not clear in all coastal areas. Dry condition during +IOD event and wet condition during LN event might cancel out the effects of rainfall and/or river discharge during +IOD_LN event. The result could be lack of clarity of rainfall and discharge patterns and ambiguity about their connection with Chl-a in coastal areas during +IOD_LN event.

3.3. The main climate event shaping the variations of Chl-a

The composite analysis revealed contrasting responses of SSHA to +sIOD (Fig. 4b) and –sIOD events (Fig. 4f) that were much more
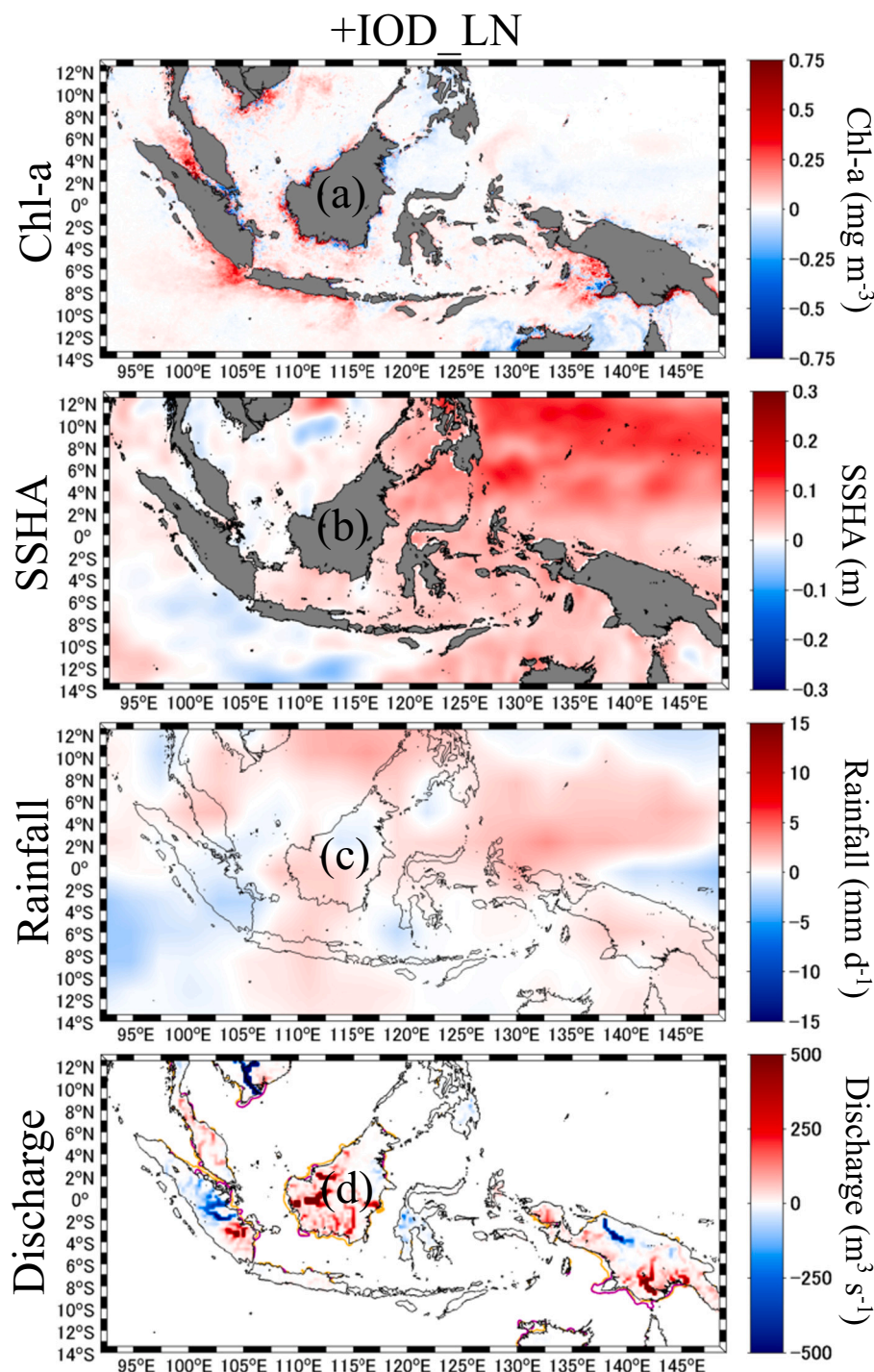
Fig. 9. (a) Map of mean Chl-a during +IOD_LN event averaged from September to December. The Chl-a was calculated by subtracting the mean Chl-a during neutral condition (2001, 2003, and 2013) from the mean Chl-a during +IOD_LN events (2007, 2008, 2011, and 2017) (see division of years based on different climate events in Fig. 2). Panels (b), (c), and (d) are the same as panel (a), but they are maps of SSHA, rainfall, and river discharge, respectively. The purple and yellow contours overlaid on the river discharge map are nLw_{555} and adg_{443} contours with values of 2.5 mW cm^{-2} μm^{-1} sr^{-1} and 0.2 m^{-1}, respectively. (For interpretation of the references to colour in this figure legend, the reader is referred to the web version of this article.)

prominent than the SSHA responses to sEN (Fig. 7b) and sLN (Fig. 7f) events. The greater SSHA responses in turn caused greater biological responses that resulted in more prominent and contrasting changes of Chl-a during +sIOD (Fig. 4a) versus −sIOD (Fig. 4e) events than during sEN (Fig. 7a) versus sLN (Fig. 7e) events. The following paragraph explains quantitatively why this contrast was especially true in the eastern Indian Ocean and the Banda Sea.

In the ocean west of Sumatra, the +sIOD (mean: 0.201 mg m^{-3}) and −sIOD (mean: −0.043 mg m^{-3}) Chl-a difference averaged 0.243 mg m^{-3}, a difference that was more than one order of magnitude larger than the difference of 0.008 mg m^{-3} between the sEN (mean: 0.012 mg m^{-3}) and sLN (mean: 0.004 mg m^{-3}) Chl-a. Similarly, in the ocean south of

Java, the +sIOD (mean: 0.165 mg m^{-3}) and −sIOD (mean: −0.178 mg m^{-3}) difference of Chl-a was 0.343 mg m^{-3}, also more than one order of magnitude larger than the difference of −0.012 mg m^{-3} between the sEN (mean: 0.065 mg m^{-3}) and sLN (mean: 0.076 mg m^{-3}) Chl-a. In the Banda Sea, the +sIOD (mean: 0.009 mg m^{-3}) and −sIOD (mean: −0.047 mg m^{-3}) Chl-a difference was 0.055 mg m^{-3}, twice the difference of 0.028 mg m^{-3} between the sEN (mean: 0.022 mg m^{-3}) and sLN (mean: −0.007 mg m^{-3}) Chl-a. Therefore, both the composite and quantitative analysis suggested that the IOD had a much greater impact on Chl-a in the eastern Indian Oceans than the ENSO did.

In contrast, in the seas of Arafura, Molucca, and north of Papua, the ENSO had only a slightly larger effect than the IOD on Chl-a. In the
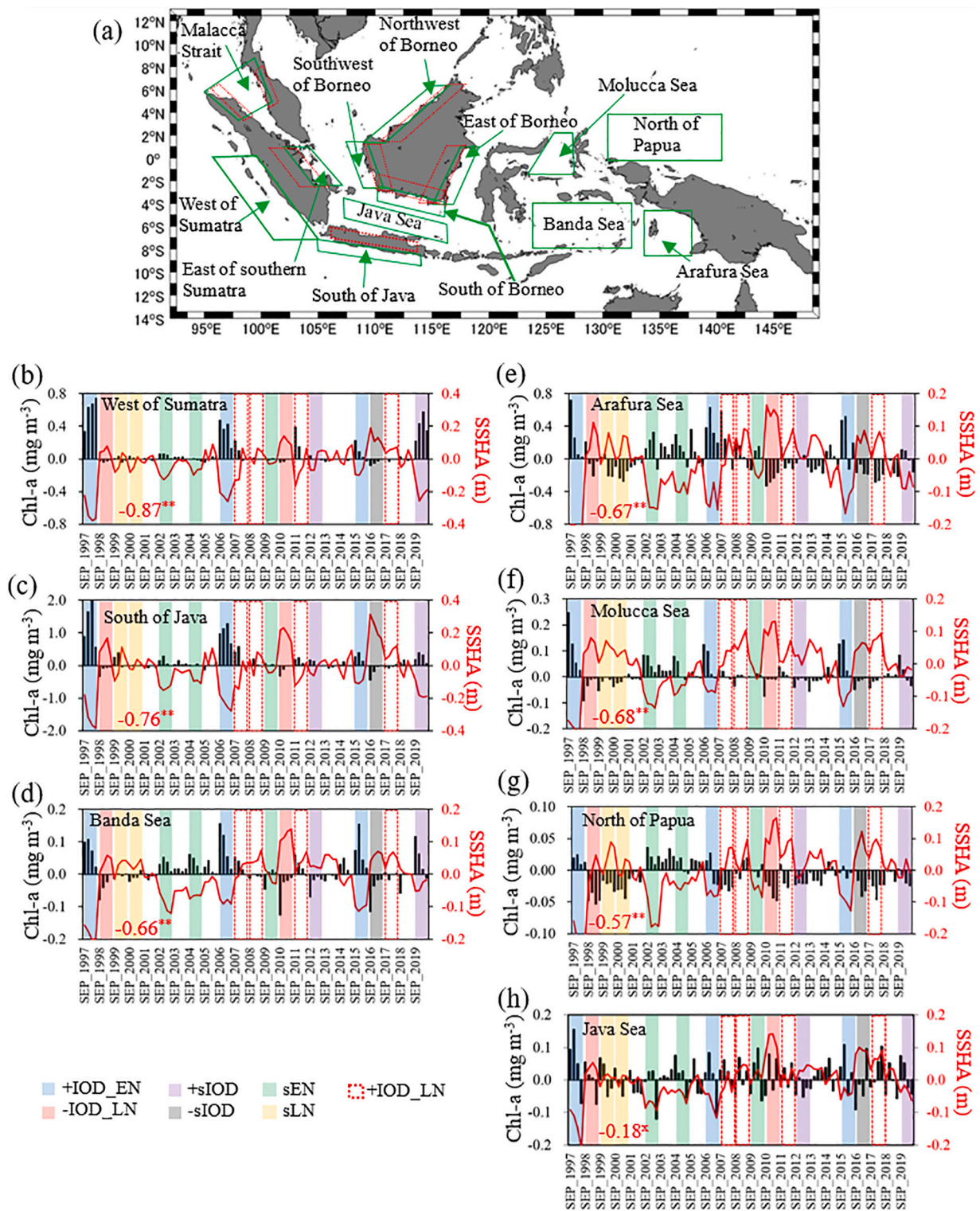
Fig. 10. (a) IMC map showing areas (green polygons) where time series of Chl-a and SSHA were derived and areas (red polygons) where time series of rainfall and river discharge were derived. Panels (b), (c), (d), (e), (f), (g), and (h) show time series (September to December 1997–2019) of Chl-a and SSHA for the areas west of Sumatra, south of Java, the Banda Sea, the Arafura Sea, the Molucca Sea, north of Papua, and the Java Sea, respectively. Vertical bars in (b–h) with different colors indicate years with different climate events. The red number shown in each graph indicates the Pearson correlation coefficient between Chl-a and SSHA. The superscript ** denotes significance level at $p < 0.001$, whereas the superscript x denotes a lack of significance ($p > 0.05$). (For interpretation of the references to colour in this figure legend, the reader is referred to the web version of this article.)
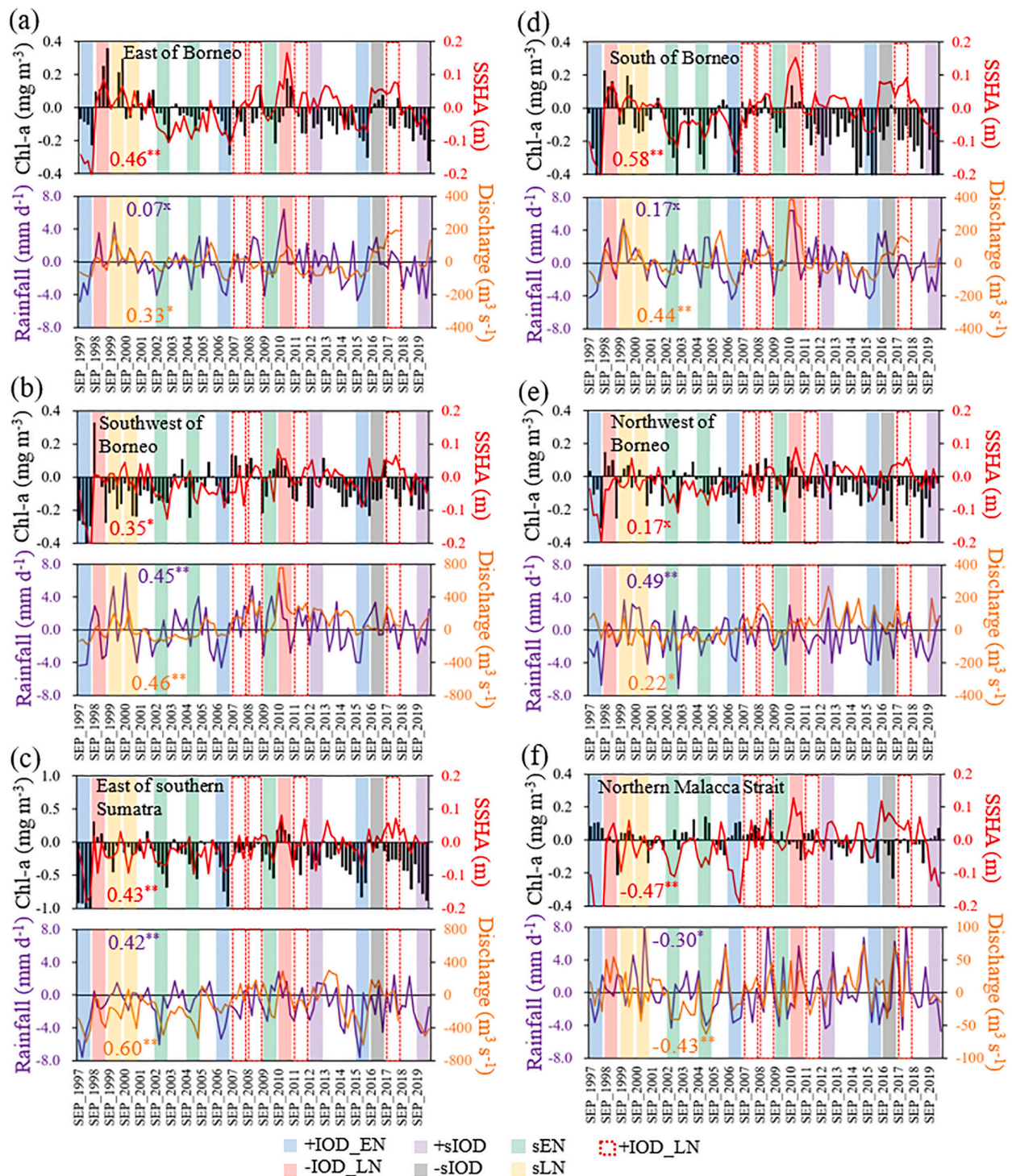
Fig. 11. Time series (September to December 1997–2019) of Chl-a and SSHA (top panels) derived from the coastal areas east of Borneo (a), southwest of Borneo (b), east of southern Sumatra (c), south of Borneo (d), northwest of Borneo (e), and the northern Malacca Strait (f). Bottom panel shows time series of rainfall and river discharge over the land(s) adjacent to the respective coastal area. Areas where Chl-a, SSHA, rainfall, and river discharge time series were calculated are mentioned in Fig. 10a. Vertical bars in (a–f) with different colors indicate years with different climate events. Red, purple, and yellow numbers shown in each graph indicate the Pearson correlation coefficients between Chl-a and the variables SSHA, rainfall, and river discharge, respectively. The superscripts ** and * denote significance at $p < 0.001$ and $p < 0.01$, respectively. The superscript ^{x} denotes a lack of significance ($p > 0.05$). (For interpretation of the references to colour in this figure legend, the reader is referred to the web version of this article.)

Arafura Sea, the sEN (mean: 0.098 mg m^{-3}) and sLN (mean: −0.138 mg m^{-3}) Chl-a difference averaged 0.236 mg m^{-3}, twice the difference of 0.147 mg m^{-3} between the +sIOD (mean: −0.007 mg m^{-3}) and −sIOD (−0.155 mg m^{-3}) Chl-a. In the Molucca Sea, the sEN (mean: 0.032 mg m^{-3}) and sLN (mean: −0.021 mg m^{-3}) Chl-a difference was 0.053 mg

m^{-3}, three times the difference of 0.019 mg m^{-3} between the +sIOD (mean: −0.001 mg m^{-3}) and −sIOD (mean: −0.021 mg m^{-3}) Chl-a. In the western Pacific Ocean north of Papua, the sEN (mean: 0.009 mg m^{-3}) and sLN (mean: −0.027 mg m^{-3}) Chl-a difference was 0.036 mg m^{-3}, six times the difference of 0.005 mg m^{-3} between +sIOD (mean:

-0.018 mg m^{-3}) and $-$sIOD (mean: -0.023 mg m^{-3}) Chl-a.

Concurrent IOD and ENSO events had the greatest impact on Chl-a to the south of Java, where the difference between +IOD_EN Chl-a (mean: 0.980 mg m^{-3}) and $-$IOD_LN Chl-a (mean: -0.131 mg m^{-3}) was 1.110 mg m^{-3}. It is likely that the low Chl-a south of Java during $-$IOD_LN event reflected mainly the impacts of $-$IOD event (Fig. 4e), because, in contrast, Chl-a tended to be high during LN event (Fig. 7e). However, the high Chl-a during LN event likely modulated the high Chl-a associated with the preceding +IOD, that is, during +IOD_LN event, as discussed above (Fig. 9a). In contrast, concurrent IOD and ENSO events had almost no impact on Chl-a in the western Pacific Ocean north of Papua. The difference of Chl-a was only 0.045 mg m^{-3} between the +IOD_EN Chl-a (mean: 0.004 mg m^{-3}) and $-$IOD_LN Chl-a (mean: -0.041 mg m^{-3}). The impact of concurrent IOD and ENSO events (i.e., the difference between +IOD_EN and $-$IOD_LN) in the eastern Indian Ocean south of Java (1.110 mg m^{-3}) was more than one order of magnitude greater than the impact in the western Pacific Ocean north of Papua (0.045 mg m^{-3}).

The great impact of +sIOD on Chl-a was apparent during the 2019 +sIOD (a strong +sIOD comparable to the 1997 +IOD, Fig. 2), when both satellite and field observations showed that the Chl-a southwest of Sumatra and Java and in Pelabuhan Ratu Bay exceeded 10.00 mg m^{-3} (Fig. 5a). An unusual bloom of photosynthetic dinoflagellates in the coastal area of Padang, West Sumatra, was also confirmed by the Indonesian Government Research Center for Marine Aquaculture in Lampung Province. High Chl-a during the 2019 +sIOD event seemed to impact fisheries production positively because there was an indication of an increase in catch landed at fishing ports during November–December 2019 along the coasts of West Sumatra and South Java, including Pasaman (West Sumatra), Pelabuhan Ratu Bay (South Java), and Bali Strait (S. Yosmeri, personal communication). The increase of the fish catch in Pasaman was also confirmed by the local fisheries authority (Indonesian Ministry of Marine Affairs and Fisheries, West Sumatra office) (S. Yosmeri, personal communication).

Sartimbul et al. (2010) reported that the *Sardinella lemuru* catch in the Bali Strait increased during the 2006 +IOD_EN event, and they argued that the increase was due mainly to the +IOD event. Our analysis thus suggested that +IOD event, whether or not coincident with EN event, was the climatic event mainly responsible for the increase of both low-trophic-level (phytoplankton) and high-trophic-level (fish) marine populations, not only in the Bali Strait but also along the coast of West Sumatra and South Java, and perhaps in the eastern archipelagic seas as well. The decreases of both low-trophic-level and high-trophic-level marine populations in the eastern Indian Ocean and archipelagic seas can thus be expected during $-$IOD event, whether or not they coincide with LN event.

The Chl-a in the northern Malacca Strait was influenced by climate variations in ways similar to the Chl-a in the eastern Indian Ocean, where upwelling/downwelling is the main factor determining variations of Chl-a related to climate events. In contrast to the northern Malacca Strait, satellite Chl-a in other coastal areas was generally low during periods of low rainfall (i.e., +sIOD, sEN, and +IOD_EN events) and high during periods of above-average rainfall (i.e., $-$sIOD, sLN, and $-$IOD_LN events). Furthermore, due to the combined effects of two events, the decline (increase) of Chl-a was remarkable during +IOD_EN ($-$IOD_LN). In many cases, such a decline (increase) of satellite Chl-a during the dry (wet) event was attributable to low (high) rainfall and/or river discharge, especially if the dry (wet) event occurred during a +IOD or +IOD_EN ($-$IOD or $-$IOD_LN) event. However, an accurate explanation for the relationship between variations of Chl-a and rainfall/discharge was sometimes obscured by riverine suspended sediment and dissolved organic matter, the presence of which compromised the accuracy of satellite Chl-a retrievals. More in-depth studies in specific coastal areas involving the development and the use of local Chl-a algorithms will be necessary to understand thoroughly the impacts of different climate events on phytoplankton Chl-a caused by variations of rainfall/discharge.

4. Conclusions

Two decades of satellite-derived Chl-a data allowed us to identify the general impacts of different climate events on the spatial variations of Chl-a in the IMC. Except for the coastal area of the northern Malacca Strait, where the variations of vertical nutrient fluxes are important, variations of riverine nutrient fluxes played an important role in determining changes of Chl-a in other coastal areas during climatic events, but careful interpretation was needed because riverine organic/inorganic matter influenced the satellite Chl-a reading. The dominant climate mode that caused Chl-a to vary shifted from the IOD in the eastern Indian Ocean to the ENSO in the western Pacific Ocean. Composite and quantitative analysis revealed that the IOD determined the variations of Chl-a in the eastern Indian Ocean to a much greater extent (more than one order of magnitude) than the ENSO did. In contrast, in the western Pacific Ocean, the effect of ENSO on variations of Chl-a was six times the effect of the IOD. Furthermore, concurrent IOD and ENSO events had the greatest impact on Chl-a in the ocean south of Java. It is likely that both low-trophic-level marine organisms such as phytoplankton and high-trophic-level marine organisms in the eastern Indian Ocean may also be more responsive to IOD event than to ENSO event.

Declaration of Competing Interest

None.

References

As-syakur, Abd.R., Adnyana, I.W.S., Mahendra, M.S., Arthana, I.W., Merit, I.N., Kasa, I.W., Ekayanti, N.W., Nuarsa, I.W., Sunarta, I.N., 2014. Observation of spatial patterns on the rainfall response to ENSO and IOD over Indonesia using TRMM Multisatellite Precipitation Analysis (TMPA). Int. J. Climatol. 34, 3825–3839. https://doi.org/10.1002/joc.3939.

Behera, S.K., Luo, J.-J., Yamagata, T., 2008. Unusual IOD event of 2007. Geophys. Res. Lett. 35, L14S11 https://doi.org/10.1029/2008GL034122.

Butler, A.H., Polvani, L.M., 2011. El Niño, La Niña, and stratospheric sudden warmings: a reevaluation in light of the observational record. Geophys. Res. Lett. 38, L13807 https://doi.org/10.1029/2011GL048084.

Chen, G., Han, W., Li, Y., Wang, D., 2016. Interannual variability of equatorial eastern Indian Ocean upwelling: local versus remote forcing. J. Phys. Oceanogr. 46, 789–807. https://doi.org/10.1175/JPO-D-15-0117.1.

Delman, A.S., Sprintall, J., McClean, J.L., Talley, L.D., 2016. Anomalous Java cooling at the initiation of positive Indian Ocean Dipole events. J. Geophys. Res. Oceans 121, 5805–5824. https://doi.org/10.1002/2016JC011635.

Horii, T., Ueki, I., Ando, K., 2013. Contrasting development and decay processes of Indian Ocean Dipoles in the 2000s. SOLA 9, 183–186. https://doi.org/10.2151/sola.2013-041.

Iskandar, I., 2010. Seasonal and interannual patterns of sea surface temperature in Banda Sea as revealed by self-organizing map. Cont. Shelf Res. 30, 1136–1148. https://doi.org/10.1016/j.csr.2010.03.003.

Iskandar, I., Rao, S.A., Tozuka, T., 2009. Chlorophyll-a bloom along the coasts of Java and Sumatra during 2006. Int. J. Remote Sens. 30 (3), 663–671. https://doi.org/10.1080/01431160802372309.

Iskandar, I., Irfan, M., Syamsuddin, F., 2013. Why was the 2008 Indian Ocean Dipole a short-lived event? Ocean Sci. J. 48 (2), 149–160. https://doi.org/10.1007/s12601-013-0012-3.

Ningsih, N.S., Rakhmaputeri, N., Harto, A.B., 2013. Upwelling variability along the southern coast of Bali and in Nusa Tenggara waters. Ocean Sci. J. 48 (1), 49–57. https://doi.org/10.1007/s12601-013-0004-3.

Nur'utami, M.N., Hidayat, R., 2016. Influences of IOD and ENSO to Indonesian rainfall variability: role of atmosphere-ocean interaction in the Indo-Pacific sector. Procedia Environ. Sci. 33, 196–203. https://doi.org/10.1016/j.proenv.2016.03.070.

Saji, N.H., Goswami, B.N., Vinayachandran, P.N., Yamadata, T., 1999. A diole mode in the tropical Indian Ocean. Nature 401, 360–363. https://doi.org/10.1038/43854.

Sari, Q.W., Utari, P.A., Setiabudidaya, D., Yustian, I., Siswanto, E., Iskandar, I., 2020. Surface chlorophyll-a variations in the Southeastern Tropical Indian Ocean during various types of positive Indian Ocean Dipole events. Int. J. Remote Sens. 41 (1), 171–184. https://doi.org/10.1080/01431161.2019.1637962.

Sartimbul, A., Nakata, H., Rohadi, E., Yusuf, B., Kadarisman, H.P., 2010. Variations in chlorophyll-a concentration and the impact on *Sardinella lemuru* cathces in Bali Strait, Indonesia. Prog. Oceanogr. 87, 168–174. https://doi.org/10.1016/j.pocean.2010.09.002.

Siswanto, E., 2015. Atmospheric deposition – another source of nutrients enhancing primary productivity in the eastern tropical Indian Ocean during positive Indian Ocean Dipole phases. Geophys. Res. Lett. 42 (13), 5378–5386. https://doi.org/10.1002/2015GL064188.

Siswanto, E., Tanaka, K., 2014. Phytoplankton biomass dynamics in the Straits of Malacca within the period of the SeaWiFS full mission: seasonal cycles, interannual variations, and decadal-scale trends. Remote Sens. 6, 2718–2742. https://doi.org/10.3390/rs6042718.

Siswanto, E., Tang, J., Yamaguchi, H., Ahn, Y.-H., Ishizaka, J., Yoo, S., Kim, S.-W., Kiyomoto, Y., Chiang, C., Kawamura, H., 2011. Empirical ocean-color algorithms to retrieve chlorophyll-a, total suspended matter, and colored dissolved organic matter absorption coefficient in the Yellow and East China Seas. J. Oceangr. 67, 627–650. https://doi.org/10.1007/s10872-011-0062-z.

Siswanto, E., Ye, H., Yamazaki, D., Tang, D., 2017. Detailed spatiotemporal impacts of El Niño on phytoplankton biomass in the South China Sea. J. Geophys. Res. Oceans 122, 2709–2723. https://doi.org/10.1002/2016JC012276.

Sprintall, J., Gordon, A.L., Koch-Larrouy, A., Lee, T., Potemra, J.T., Pujiana, K., Wijffels, S.E., 2014. The Indonesian Seas and their impact on the Coupled Ocean Climate System. Nat. Geosci. 7, 487–492. https://doi.org/10.1038/NGEO2188.

Sun, C., 2017. Riverine influence on ocean color in the equatorial South China Sea. Cont. Shelf Res. 143, 151–158. https://doi.org/10.1016/j.csr.2016.10.008.

Susanto, R.D., Marra, J., 2005. Effect of the 1997/98 El Niño on chlorophyll a variability along the southern coasts of Java and Sumatra. Oceanogr. 18 (4), 124–127. https://doi.org/10.5670/oceanog.2005.13.

Susanto, R.D., Gordon, A.L., Zheng, Q., 2001. Upwelling along the coasts of Java and Sumatra and its relation to ENSO. Geophys. Res. Lett. 28 (8), 1559–1602. https://doi.org/10.1029/2000GL011844.

Susanto, R.D., Moore II, T.M., Marra, J., 2006. Ocean color variability in the Indonesian Seas during the SeaWiFS era. Geochem. Geophys. Geosyst. 7 (5) https://doi.org/10.1029/2005GC001009.

Susanto, R.D., Field, A., Gordon, A.L., Adi, T.R., 2012. Variability of Indonesia throughflow within Makassar Strait, 2004–2009. J. Geophys. Res. Oceans 117, C09013. https://doi.org/10.1029/2012JC008096.

Tan, C.K., Ishizaka, J., Matsumura, S., Yusoff, F.M., Mohamed, M.I.H., 2006. Seasonal variability of SeaWiFS chlorophyll a in the Malacca Straits in relation to Asian monsoon. Cont. Shelf Res. 26, 168–178. https://doi.org/10.1016/j.csr.2005.09.008.

Wilson, C., Adamec, D., 2001. Correlations between surface chlorophyll and sea surface height in the tropical Pacific Ocean during the 1997–1999 El Niño–Southern Oscillation event. J. Geophys. Res. 106 (C12), 31175–31188. https://doi.org/10.1029/2000JC000724.

Zhang, L., Du, Y., Cai, W., 2018. A spurious positive Indian Ocean Dipole in 2017. Sci. Bull. 63, 1170–1172. https://doi.org/10.1016/j.scib.2018.08.001.